

A 19-Point Average-derivative Optimal Scheme for 3D Frequency-domain Scalar Wave Equation

Jing-Bo Chen*

Key Laboratory of Petroleum Resources Research, Institute of Geology and Geophysics, Chinese Academy of Sciences, China

Abstract

A 27-point optimal scheme for 3D frequency-domain scalar wave equation was recently developed. This scheme includes 9 optimization coefficients, and is relatively complicated. To simplify this scheme, a 19-point average-derivative optimal scheme for 3D frequency-domain scalar wave equation is constructed in this paper. This new 19-point scheme includes only 5 optimization coefficients, but maintains similar advantages of the 27-point optimal scheme. Compared to the classical 7-point scheme, the number of grid points per shortest wavelength is reduced from approximately 13 to approximately 4 by this 19-point optimal scheme for equal directional sampling intervals and unequal directional sampling intervals as well. Two numerical examples are presented to demonstrate the theoretical analysis.

Keywords: Seismic modeling; Frequency domain; Three dimension; Average derivative; Optimization

Introduction

Full waveform inversion (FWI) is a full-wavefield-modeling-based data-fitting process to extract structural information of subsurface from seismograms [1]. FWI can be implemented either in time-domain [2-4] or in frequency-domain [5-7].

Forward modeling is an important part of FWI. In line with FWI, forward modeling can be divided into two categories: time-domain modeling and frequency-domain modeling. Compared to time-domain modeling [8], frequency-domain modeling has its advantages: convenient manipulations of a single frequency, multi-shot computation based on a direct solver, and easy implementation of attenuation [9]. In addition, no wavefield-storage issue occurs when constructing the gradient of FWI for frequency-domain modeling. This is not the case when constructing the gradient of FWI for time-domain modeling. This is because the forward source wavefield and backward receiver wavefield are computed in opposite time direction [10,11].

The main disadvantage of frequency-domain modeling is that it can only be performed in an implicit way by solving a set of linear equations. In comparison with the time-domain modeling, this disadvantage is particularly obvious when it comes to 3D computation. Therefore, reducing the number of grid points per shortest wavelength is in great demand in particular when direct solution techniques are employed. Using a rotated coordinate system, Jo et al. [9] developed a 9-point optimal scheme for 2D scalar wave equation. This 9-point scheme reduces the number of grid points per wavelength to approximately 4, and leads to significant reductions of computer memory and CPU time. Hustadt et al. [12] and Operto et al. [13] generalized the rotated-coordinate method to variable density case and 3D case, respectively.

To overcome the disadvantage of the rotated optimal 9-point scheme, Chen [14] developed a new 9-point finite-difference scheme for 2D scalar wave equation based on an average-derivative approach [15,16]. This new scheme imposes no restriction of equal directional sampling intervals, and reduces the number of grid points per shortest wavelength to approximately 4 for both equal and unequal directional sampling intervals. Chen [17] further generalized the average-derivative method and developed a 27-point optimal scheme for 3D scalar wave equation. Compared to the classical 7-point scheme, the number of grid points per shortest wavelength is reduced from approximately 13 to approximately 4 by this 27-point optimal scheme for both equal and

unequal directional sampling intervals within the relative phase error of one percent.

The 27-point scheme Chen [17] includes 9 optimization coefficients, and has a relatively high complexity. By reducing the number of optimization coefficients from 9 to 5, a simplified 19-point average-derivative optimal scheme for 3D scalar wave equation can be achieved. In the next section, I will present this new 19-point scheme. This is followed by the optimization of coefficients and a numerical dispersion analysis. Numerical examples are then presented to demonstrate the theoretical analysis.

A 19-Point Scheme for 3D Wave Equation

The 3D frequency-domain scalar wave equation can be written as

$$\frac{\partial^2 P}{\partial x^2} + \frac{\partial^2 P}{\partial y^2} + \frac{\partial^2 P}{\partial z^2} + \frac{\omega^2}{v^2} P = 0, \quad (1)$$

where P is the pressure wavefield, ω is the angular frequency, and $v(x, y, z)$ is the velocity.

An average-derivative optimal 19-point scheme for equation (1) can be obtained as follows (Figure 1):

$$\begin{aligned} & \frac{\bar{P}_{m+1,l,n} - 2\bar{P}_{m,l,n} + \bar{P}_{m-1,l,n}}{\Delta x^2} + \frac{\hat{P}_{m,l+1,n} - 2\hat{P}_{m,l,n} + \hat{P}_{m,l-1,n}}{\Delta y^2} \\ & + \frac{\tilde{P}_{m,l,n+1} - 2\tilde{P}_{m,l,n} + \tilde{P}_{m,l,n-1}}{\Delta z^2} + \frac{\omega^2}{v_{m,l,n}^2} (cP_{m,l,n} + dA + eB) = 0, \end{aligned} \quad (2)$$

where

$$\bar{P}_{r,l,n} = \alpha(P_{r,l+1,n} + P_{r,l,n+1} + P_{r,l-1,n} + P_{r,l,n-1}) + (1-4\alpha)P_{r,l,n}, \quad r = m+1, m, m-1,$$

$$\hat{P}_{m,s,n} = \beta(P_{m+1,s,n} + P_{m,s,n+1} + P_{m-1,s,n} + P_{m,s,n-1}) + (1-4\beta)P_{m,s,n}, \quad s = l+1, l, l-1,$$

***Corresponding author:** Chen JB, Key Laboratory of Petroleum Resources Research, Institute of Geology and Geophysics, Chinese Academy of Sciences, China, Tel: +86-010-82998156; E-mail: chenjb@mail.igcas.ac.cn

Received October 30, 2014; **Accepted** December 20, 2014; **Published** December 27, 2014

Citation: Chen JB (2015) A 19-Point Average-derivative Optimal Scheme for 3D Frequency-domain Scalar Wave Equation. J Geophys Remote Sensing 4: 140. doi: 10.4172/2169-0049.1000140

Copyright: © 2015 Chen JB. This is an open-access article distributed under the terms of the Creative Commons Attribution License, which permits unrestricted use, distribution, and reproduction in any medium, provided the original author and source are credited.

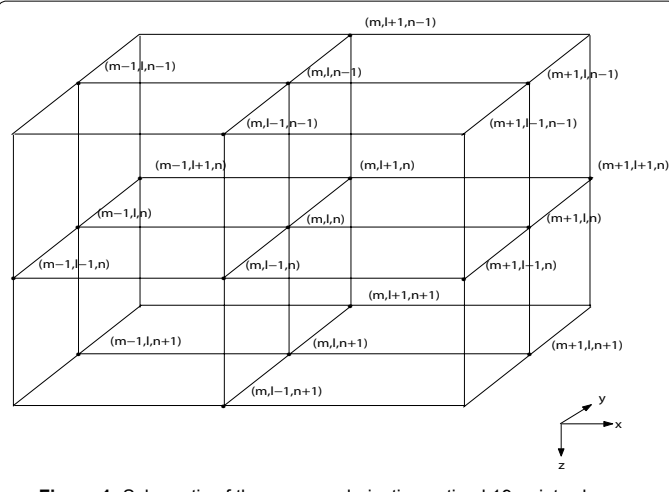


Figure 1: Schematic of the average-derivative optimal 19-point scheme.

$$\begin{aligned} \tilde{P}_{m,l,q} &= \gamma(P_{m+1,l,q} + P_{m,l+1,q} + P_{m-1,l,q} + P_{m,l-1,q}) + (1-4\gamma)P_{m,l,q}, \quad q = n+1, n, n-1, \\ A &= (P_{m,l+1,n} + P_{m,l,n+1} + P_{m,l-1,n} + P_{m,l,n-1} + P_{m+1,l,n} + P_{m-1,l,n}), \\ B &= (P_{m+1,l+1,n} + P_{m+1,l,n+1} + P_{m+1,l-1,n} + P_{m+1,l,n-1} + P_{m-1,l+1,n} + P_{m-1,l,n+1} \\ &\quad + P_{m-1,l-1,n} + P_{m-1,l,n-1} + P_{m,l+1,n+1} + P_{m,l-1,n+1} + P_{m,l+1,n-1} + P_{m,l-1,n-1}), \end{aligned}$$

where α , β , γ , c , and d are coefficients which are to be optimized, and $e = \frac{1-c-6d}{12}$.

Here, $P_{m,l,n} \approx P(m\Delta x, l\Delta y, n\Delta z)$, $v_{m,l,n} \approx v(m\Delta x, l\Delta y, n\Delta z)$, and Δx , Δy , and Δz are directional sampling intervals in the x-direction, y-direction and z-direction, respectively.

In equation (2), the approximation of the derivative in one direction involves an average of wavefield values from remaining two directions. In this way, a family of approximations to the derivative is obtained, which depends on a free parameter (α , β , or γ). The free parameters c and d from the average of the mass acceleration term play the same role. Therefore, based on optimization techniques, the optimization approximation can be chosen to reduce dispersion errors. The average-derivative optimal 19-point scheme (2) also includes the classical 7-point scheme as a special case, because when $\alpha=0$, $\beta=0$, $\gamma=0$, $c=1$, and $d=0$, the scheme (2) reduces to the classical 7-point scheme:

$$\begin{aligned} &\frac{P_{m+1,l,n} - 2P_{m,l,n} + P_{m-1,l,n}}{\Delta x^2} + \frac{P_{m,l+1,n} - 2P_{m,l,n} + P_{m,l-1,n}}{\Delta y^2} \\ &+ \frac{P_{m,l,n+1} - 2P_{m,l,n} + P_{m,l,n-1}}{\Delta z^2} + \frac{\omega^2}{v_{m,l,n}^2} P_{m,l,n} = 0. \end{aligned} \quad (3)$$

Optimization and Dispersion Analysis

Substituting $P(x, y, z, \omega) = P_0 e^{i(k_x x + k_y y + k_z z)}$ into equation (2) and assuming a constant v , one obtains the discrete dispersion relation

$$\frac{\omega^2}{v^2} = \frac{2(1-\cos(k_x \Delta x))E_x + 2r_1^2(1-\cos(k_y \Delta y))E_y + 2r_2^2(1-\cos(k_z \Delta z))E_z}{\Delta x^2(c + 2d\tilde{A} + 4e\tilde{B})}, \quad (4)$$

where

$$Ex = 2\alpha(\cos(k_y \Delta y) + \cos(k_z \Delta z)) + (1-4\alpha),$$

$$\begin{aligned} Ez &= 2\gamma(\cos(k_x \Delta x) + \cos(k_y \Delta y)) + (1-4\gamma), \\ r_1 &= \frac{\Delta x}{\Delta y}, r_2 = \frac{\Delta x}{\Delta z}, \quad \tilde{A} = \cos(k_x \Delta x) + \cos(k_y \Delta y) + \cos(k_z \Delta z), \end{aligned} \quad (5)$$

$$\tilde{B} = \cos(k_x \Delta x) \cos(k_y \Delta y) + \cos(k_x \Delta x) \cos(k_z \Delta z) + \cos(k_y \Delta y) \cos(k_z \Delta z).$$

From equation (4), one can obtain the normalized phase velocity

$$\frac{V_{ph}}{v} = \frac{\left[2 \left[1 - \cos \left(\frac{2\pi \sin \theta \cos \phi}{G} \right) \right] Ex + 2r_1^2 \left[1 - \cos \left(\frac{2\pi \sin \theta \sin \phi}{r_1 G} \right) \right] Ey + 2r_2^2 \left[1 - \cos \left(\frac{2\pi \cos \theta}{r_2 G} \right) \right] Ez \right]^{\frac{1}{2}}}{\frac{2\pi}{G} \{c + 2d\tilde{A} + 4e\tilde{B}\}^{\frac{1}{2}}}, \quad (6)$$

where V_{ph} is the phase velocity, $k_x = k \sin \theta \cos \phi$, $k_y = k \sin \theta \sin \phi$, $k_z = k \cos \theta$, $G = \frac{2\pi}{k \Delta x}$, θ is the propagation angle, ϕ is the azimuth angle, and

$$\begin{aligned} Ex &= 2\alpha \left(\cos \left(\frac{2\pi \sin \theta \sin \phi}{r_1 G} \right) + \cos \left(\frac{2\pi \cos \theta}{r_2 G} \right) \right) + (1-4\alpha), \\ Ez &= 2\beta \left(\cos \left(\frac{2\pi \sin \theta \cos \phi}{G} \right) + \cos \left(\frac{2\pi \cos \theta}{r_2 G} \right) \right) + (1-4\beta), \\ E_z &= 2\gamma \left(\cos \left(\frac{2\pi \sin \theta \cos \phi}{G} \right) + \cos \left(\frac{2\pi \sin \theta \sin \phi}{r_1 G} \right) \right) + (1-4\gamma), \\ \tilde{A} &= \cos \left(\frac{2\pi \sin \theta \cos \phi}{G} \right) + \cos \left(\frac{2\pi \sin \theta \sin \phi}{r_1 G} \right) + \cos \left(\frac{2\pi \cos \theta}{r_2 G} \right), \\ \tilde{B} &= \cos \left(\frac{2\pi \sin \theta \cos \phi}{G} \right) \cos \left(\frac{2\pi \sin \theta \sin \phi}{r_1 G} \right) + \cos \left(\frac{2\pi \sin \theta \cos \phi}{G} \right) \cos \left(\frac{2\pi \cos \theta}{r_2 G} \right) \\ &\quad + \cos \left(\frac{2\pi \sin \theta \sin \phi}{r_1 G} \right) \cos \left(\frac{2\pi \cos \theta}{r_2 G} \right). \end{aligned} \quad (7)$$

The coefficients α , β , γ , c , and d are obtained by minimizing the phase error:

$$PE = \int \int \int \left[1 - \frac{V_{ph}(\theta, \phi, \tilde{k}; \alpha, \beta, \gamma, c, d)}{v} \right]^2 d\tilde{k} d\theta d\phi, \quad (8)$$

$$\text{where } \tilde{k} = \frac{1}{G}.$$

The optimization coefficients for different $r_1 = \frac{\Delta_x}{\Delta_y}$ and $r_2 = \frac{\Delta_x}{\Delta_z}$ when $\Delta z = \max\{\Delta x, \Delta y, \Delta z\}$ are listed in Table 1. The optimization coefficients for the cases where $\Delta y = \max\{\Delta x, \Delta y, \Delta z\}$, and $\Delta z = \max\{\Delta x, \Delta y, \Delta z\}$ are listed in Tables 2 and 3, respectively.

Now I perform numerical dispersion analysis. First, I consider the case where $r1=1$ and $r2=1$, which corresponds to the equal directional intervals $\Delta x=\Delta y=\Delta z$. Figure 2 shows normalized phase velocity curves of the classical 7-point scheme (3) and the average-derivative optimal 19-point scheme (2) for fixed azimuth angle ϕ and different propagation angles θ . Figure 3 shows normalized phase velocity curves of the classical 7-point scheme (3) and the average-derivative optimal 19-point scheme (2) for fixed propagation angle θ and different azimuth angles ϕ . From these figures, one can conclude that within the phase velocity error of 1%, the classical 7-point scheme (3) requires approximately 13 grid points per shortest wavelength, while the average-derivative optimal 19-point scheme (2) requires approximately 4 points.

In order to obtain an overall estimation of the phase velocity errors varying with ϕ and θ , the following relative phase velocity error is considered:

	α	β	γ	c	d
$r_1=1$	0.100063	0.100063	0.100522	0.454208	0.090965
$r_2=1$					
$r_1=1$	0.098871	0.098869	0.095057	0.458533	0.090244
$r_2=2$					
$r_1=1$	0.100411	0.100411	0.093990	0.455768	0.090705
$r_2=3$					
$r_1=2$	0.100501	0.095894	0.101605	0.453894	0.091018
$r_2=1$					
$r_1=2$	0.075550	0.098454	0.099177	0.462434	0.089594
$r_2=2$					
$r_1=2$	0.078754	0.100805	0.096196	0.457813	0.090364
$r_2=3$					
$r_1=3$	0.099743	0.094440	0.103178	0.453663	0.091056
$r_2=1$					
$r_1=3$	0.065131	0.095610	0.103061	0.461432	0.089761
$r_2=2$					
$r_1=3$	0.085513	0.0961245	0.096437	0.456674	0.090554
$r_2=3$					

Table 1: Optimization coefficients for α , β , γ , c , and d for different $r_1 = \frac{\Delta x}{\Delta y}$ and $r_2 = \frac{\Delta x}{\Delta z}$ when $\Delta x = \max\{\Delta x, \Delta y, \Delta z\}$.

	α	β	γ	c	d
$r_1=1$	0.100063	0.100063	0.100522	0.454208	0.090965
$r_2=1$					
$r_1=1$	0.098871	0.098869	0.095057	0.458533	0.090244
$r_2=2$					
$r_1=1$	0.100411	0.100411	0.093990	0.455768	0.090705
$r_2=3$					
$r_1=2$	0.095894	0.100501	0.101605	0.453894	0.091018
$r_2=1$					
$r_1=2$	0.098454	0.075550	0.099177	0.462434	0.089594
$r_2=2$					
$r_1=2$	0.100805	0.078754	0.096196	0.457813	0.090364
$r_2=3$					
$r_1=3$	0.094440	0.099743	0.103178	0.453663	0.091056
$r_2=1$					
$r_1=3$	0.095610	0.065131	0.103061	0.461432	0.089761
$r_2=2$					
$r_1=3$	0.0961245	0.085513	0.096437	0.456674	0.090554
$r_2=3$					

Table 2: Optimization coefficients for α , β , γ , c , and d for different $r_1 = \frac{\Delta y}{\Delta x}$ and $r_2 = \frac{\Delta y}{\Delta z}$ when $\Delta y = \max\{\Delta x, \Delta y, \Delta z\}$.

$$RE = \left| \frac{V_{ph}(\phi, \theta, \frac{1}{G}) - v}{v} \right|, \quad 0^\circ \leq \phi \leq 180^\circ, \quad 0^\circ \leq \theta \leq 90^\circ. \quad (9)$$

Figure 4 shows the relative phase velocity errors for the classical 7-point scheme and the average-derivative optimal 19-point scheme for different r_1 . With increasing r_1 , the relative phase velocity errors for the classical 7-point scheme increase. On the other hand, the relative phase velocity errors for the classical average-derivative optimal 19-point scheme are within 1% as $\frac{1}{G}$ increases.

Figures 5-7 show the results for the case where $r_1=1$ and $r_2=2$. In this case, one can draw the same conclusion: within the phase velocity

error of 1% and for equal and unequal directional sampling intervals, the classical 7-point scheme (3) requires approximately 13 grid points per shortest wavelength, while the average-derivative optimal 19-point scheme (2) requires approximately 4 grid points. For other cases on r_1 and r_2 , similar analysis can be made.

Numerical Examples

In this section, two numerical examples are presented to verify the theoretical analysis on the classical 7-point scheme (3) and the average-derivative optimal 19-point scheme (2). First, I consider a homogeneous velocity model with a velocity of 4000 m/s (Figure 8a). Horizontal and vertical distances are $x=2$ km, $y=2$ km, and $z=1$ km, respectively. A Ricker wavelet is placed at the center of the model as a source. The receivers are placed at a depth of 250 m. PML absorbing boundary conditions are applied along the edges of the model. In this numerical example, a monochromatic wavefield of 20 Hz is computed. According to the criterion of 4 grid points per smallest wavelength, horizontal sampling interval is determined by $\Delta x = 4000/20/4 = 50$ m. Set $\Delta y = \Delta x$ and $\Delta z = \Delta x/2$. Accordingly, horizontal and vertical samplings are $\Delta x = \Delta y = \Delta z = 41$. In this case, the optimization coefficients for the average-derivative optimal 19-point scheme (2) are $\alpha=0.098871$, $\beta=0.098869$, $\gamma=0.095057$, $c=0.458533$, and $d=0.090244$. In this example, analytical solution is available to make comparisons with numerical solutions. For the analytical solution, the following formula is used

$$P(x, y, z, \omega) = \frac{1}{r} \exp \left\{ i\omega \frac{r}{v} \right\} \mp F(\omega), \quad (10)$$

where F is the Fourier transformation of the Ricker wavelet, and

$$r = \sqrt{(x - x_0)^2 + (y - y_0)^2 + (z - z_0)^2},$$

where (x_0, y_0, z_0) is the source position.

Figure 8b shows the real part of the 20 Hz monochromatic wavefield computed with the analytical formula (10), the classical 7-point scheme (3) and the average-derivative optimal 19-point scheme (2). The simulation result with the average-derivative optimal 19-point scheme (2) is in good agreement with the analytical result while the result with

	α	β	γ	c	d
$r_1=1$	0.100063	0.100063	0.100522	0.454208	0.090965
$r_2=1$					
$r_1=1$	0.100501	0.095894	0.101605	0.453894	0.091018
$r_2=2$					
$r_1=1$	0.099743	0.094440	0.103178	0.453663	0.091056
$r_2=3$					
$r_1=2$	0.095894	0.100501	0.101605	0.453894	0.091018
$r_2=1$					
$r_1=2$	0.098874	0.098875	0.092663	0.454047	0.090992
$r_2=2$					
$r_1=2$	0.100216	0.096648	0.089797	0.453817	0.091030
$r_2=3$					
$r_1=3$	0.094440	0.099743	0.103178	0.453663	0.091056
$r_2=1$					
$r_1=3$	0.096648	0.100216	0.089797	0.453817	0.091030
$r_2=2$					
$r_1=3$	0.097303	0.097303	0.088657	0.453614	0.091064
$r_2=3$					

Table 3: Optimization coefficients for α , β , γ , c , and d for different $r_1 = \frac{\Delta z}{\Delta x}$ and $r_2 = \frac{\Delta z}{\Delta y}$ when $\Delta z = \max\{\Delta x, \Delta y, \Delta z\}$.

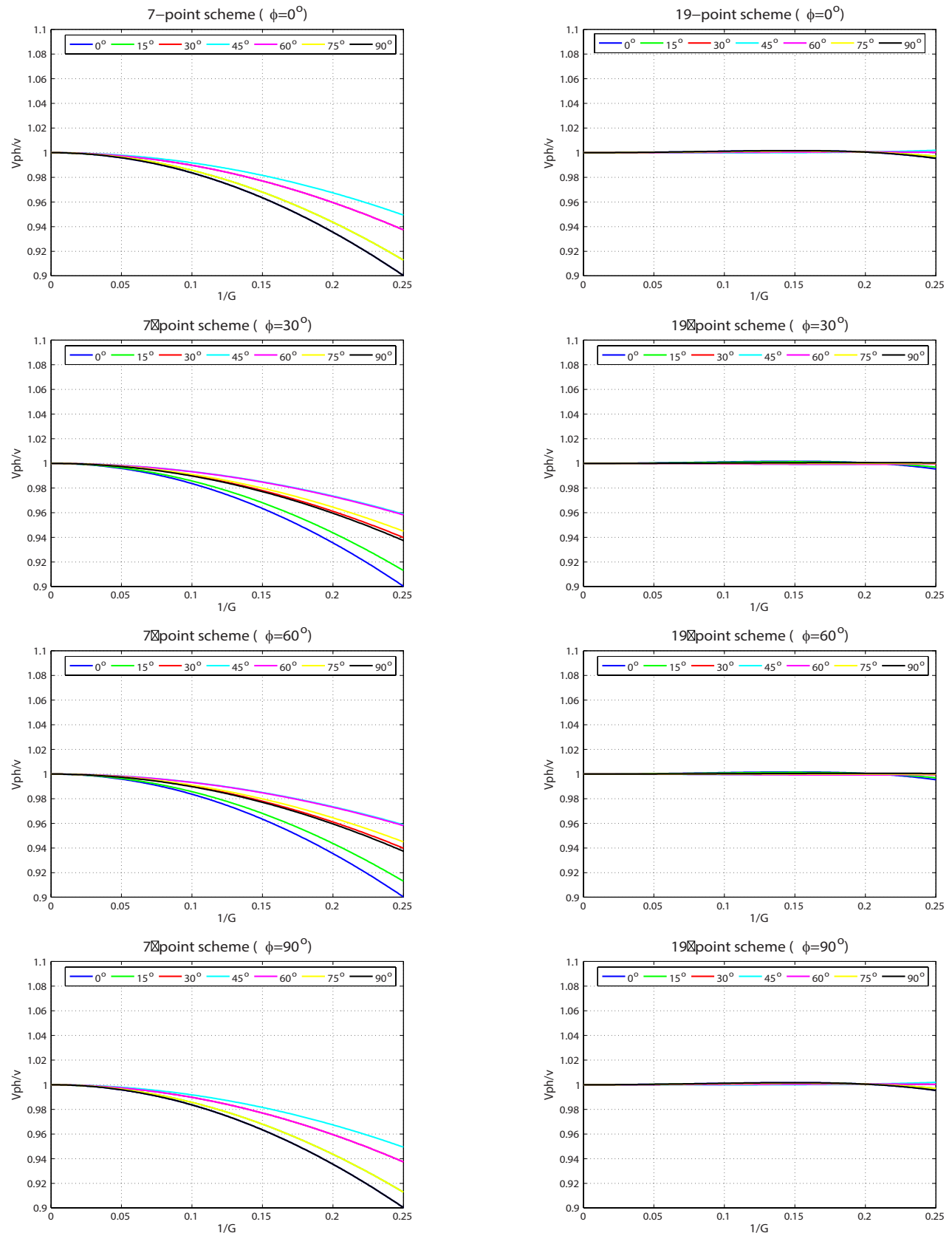


Figure 2: Normalized phase velocity curves of the classical 7-point scheme and the average-derivative optimal 19-point scheme for fixed azimuth angle ϕ and different propagation angles θ when $r_1 = 1$ and $r_2 = 1$.

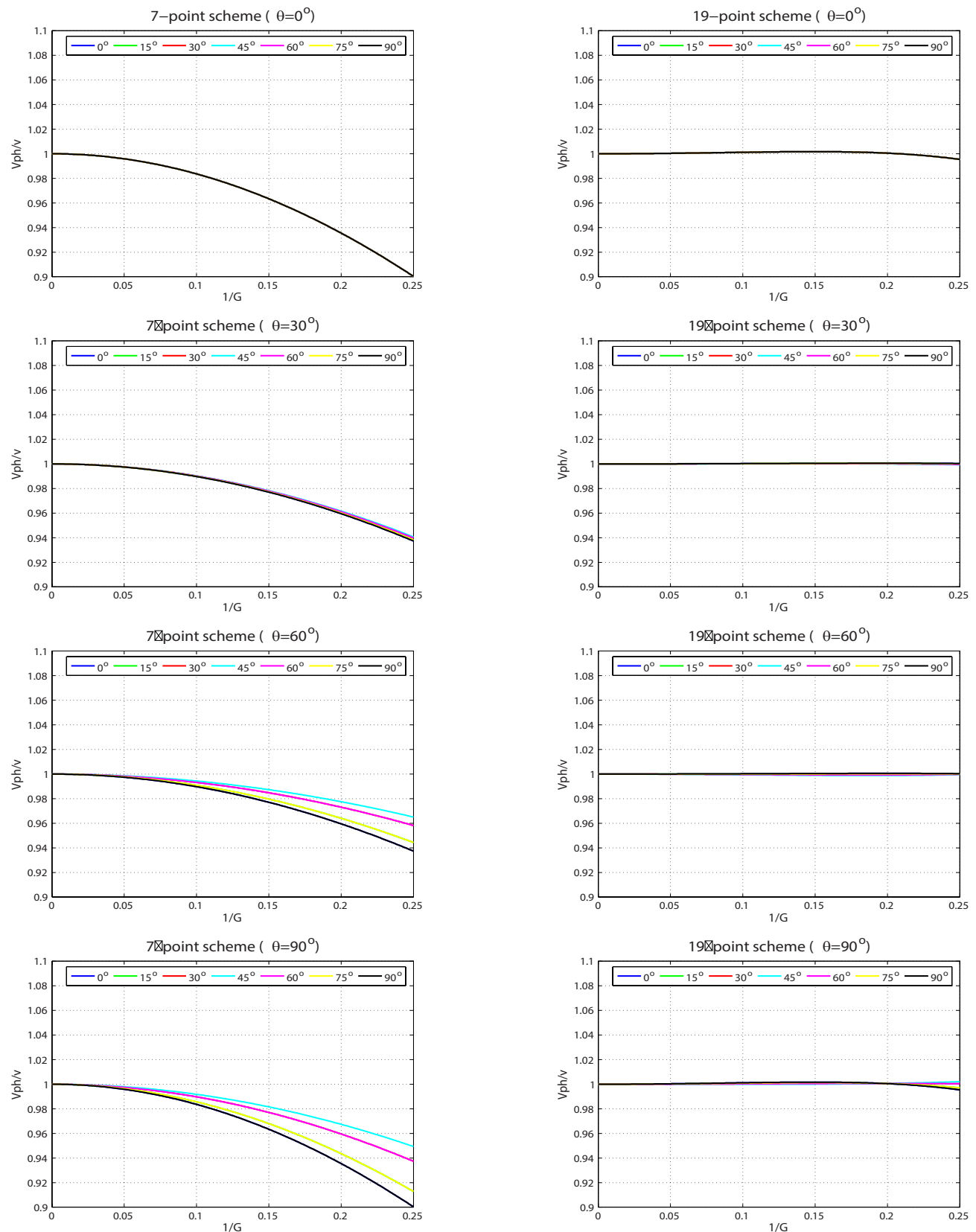


Figure 3: Normalized phase velocity curves of the classical 7-point scheme and the average-derivative optimal 19-point scheme for fixed propagation angle θ and different azimuth angles ϕ when $r_1 = 1$ and $r_2 = 1$.

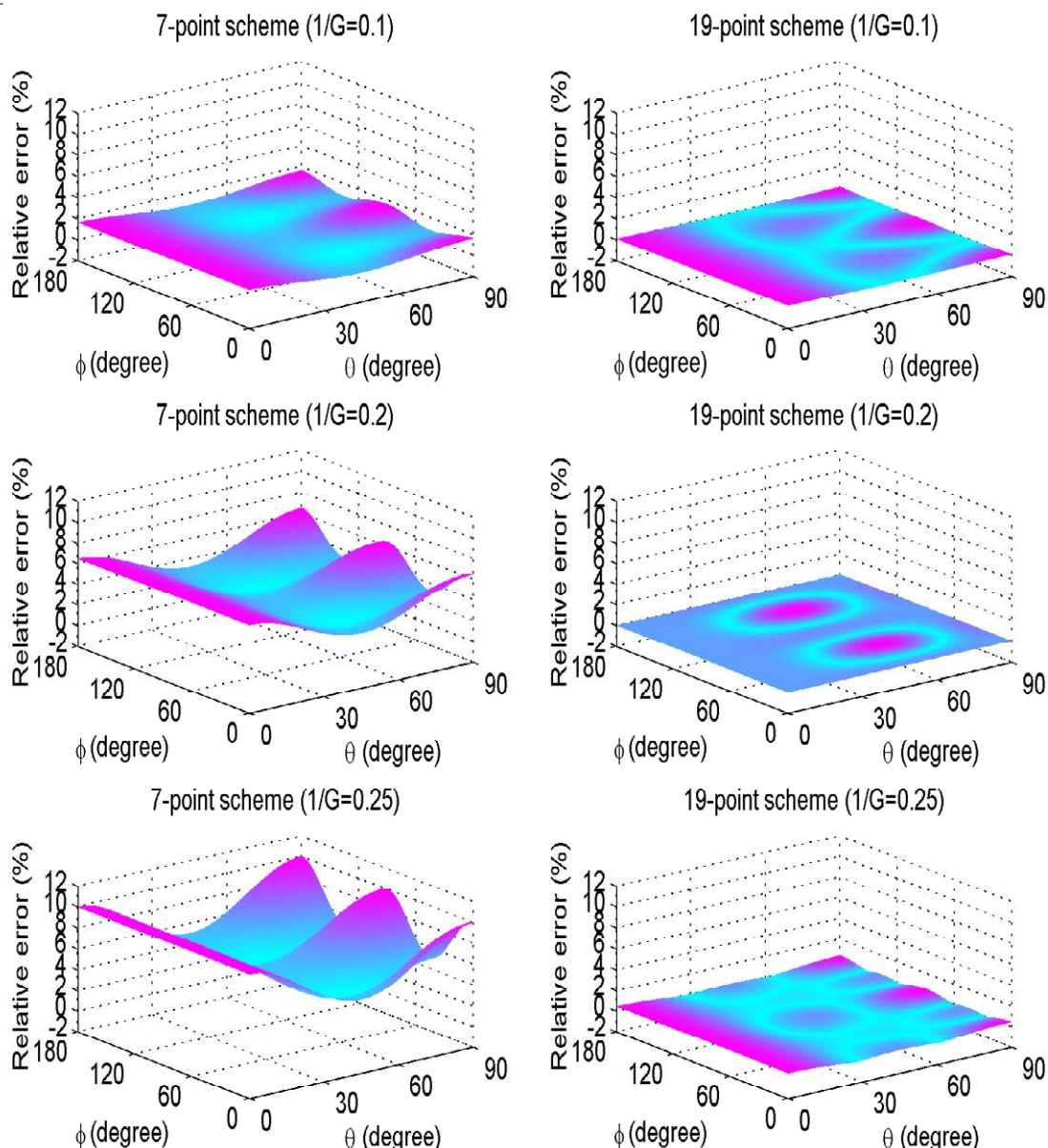
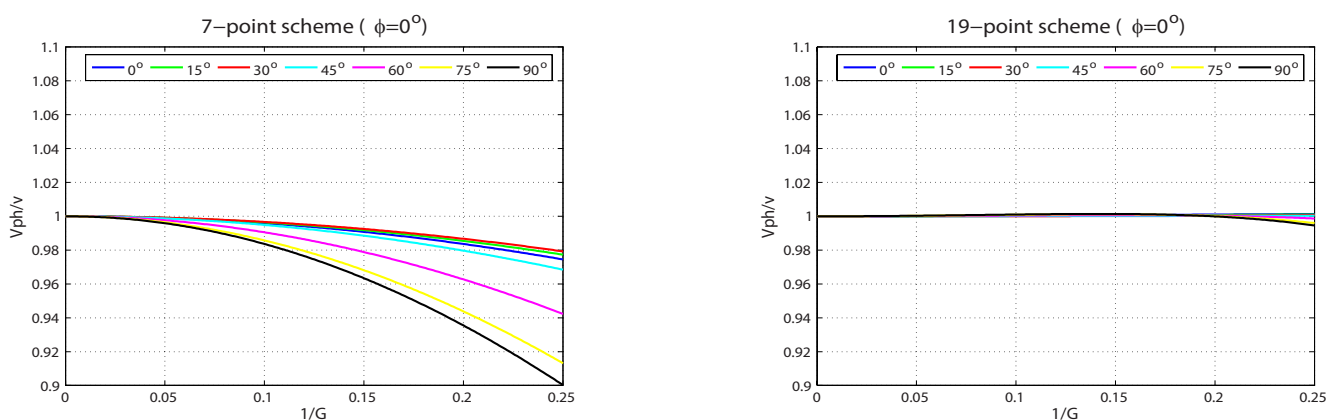


Figure 4: The relative phase velocity errors for the classical 7-point scheme and the average-derivative optimal 19-point scheme for different $1/G$ where $r_1=1$ and $r_2=1$.



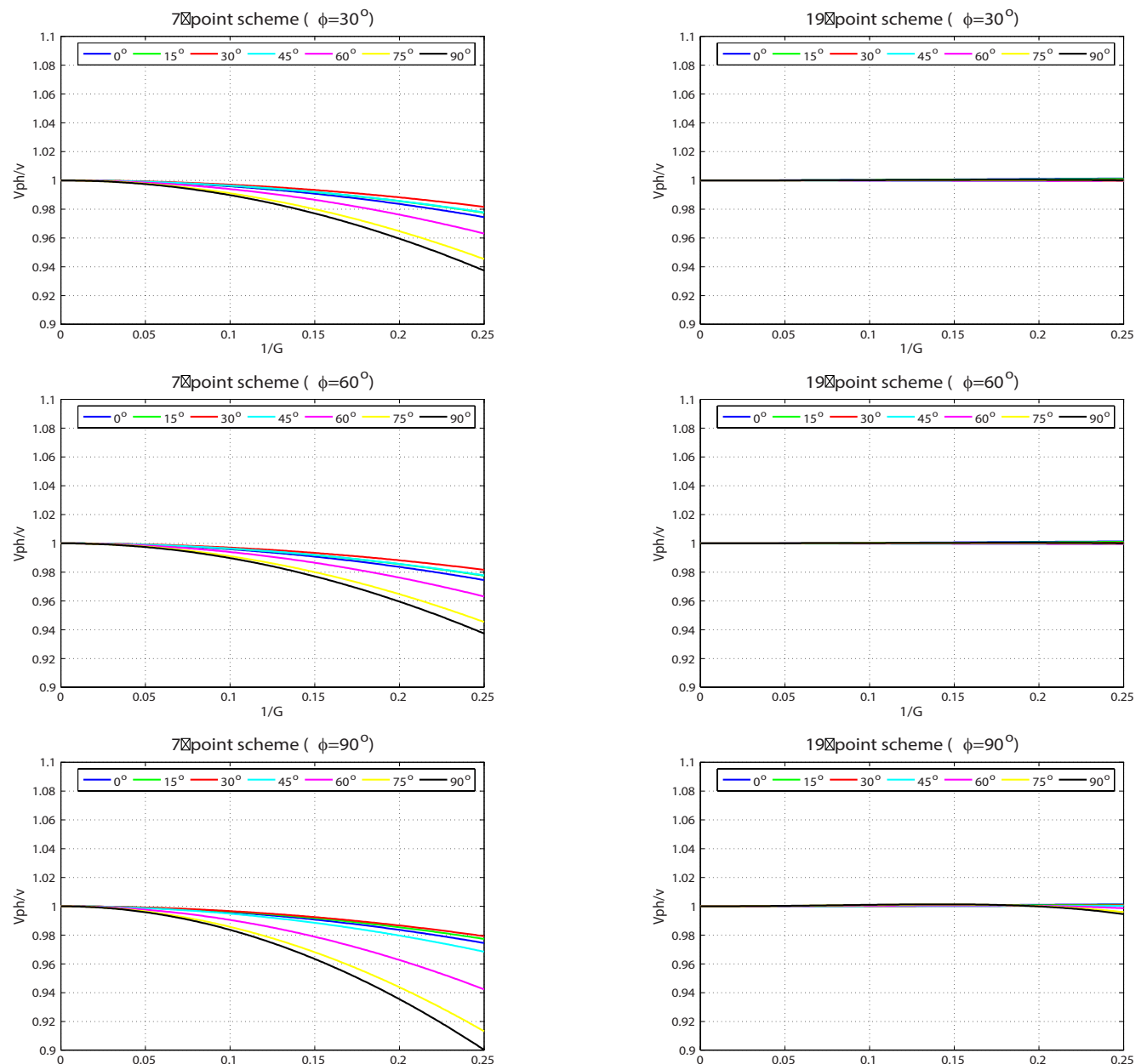


Figure 5: Normalized phase velocity curves of the classical 7-point scheme and the average-derivative optimal 19-point scheme for fixed azimuth angle ϕ and different propagation angles θ when $r_1 = 1$ and $r_2 = 2$.

the classical 7-point scheme (3) exhibits large errors due to numerical dispersion.

Second, I consider a heterogeneous velocity model. Figure 9a shows a salt dome velocity model. The velocity of the salt dome is 5000 m/s, and the velocity of the overburden is 4000 m/s. The distances, sampling numbers, the Ricker wavelet, and the frequency used in this example are the same as those used in the homogeneous velocity model. For the top boundary, a free-surface condition is used, and for other edges of the model, PML absorbing boundary conditions are applied. The source is located at a depth of 200 m, and the receivers are placed immediately under the free surface. In this example, analytical solution is not available. Therefore, I consider the 27-point optimal scheme in Chen [17] for a comparison. Figure 9b shows the real part of the 20

Hz monochromatic wavefield computed with the 27-point optimal scheme, the classical 7-point scheme (3) and the average-derivative optimal 19-point scheme (2). The simulation result with the average-derivative optimal 19-point scheme (2) is in good agreement with the result of the 27-point scheme. On the other hand, the result with the classical 7-point scheme (3) exhibits large discrepancies with the result of the 27-point scheme due to numerical dispersion.

Conclusions

To simplify the 27-point optimal scheme, a 19-point average-derivative optimal scheme for 3D frequency-domain scalar wave equation is developed. The optimization coefficients are obtained by minimizing the phase velocity errors, and they vary with the ratios

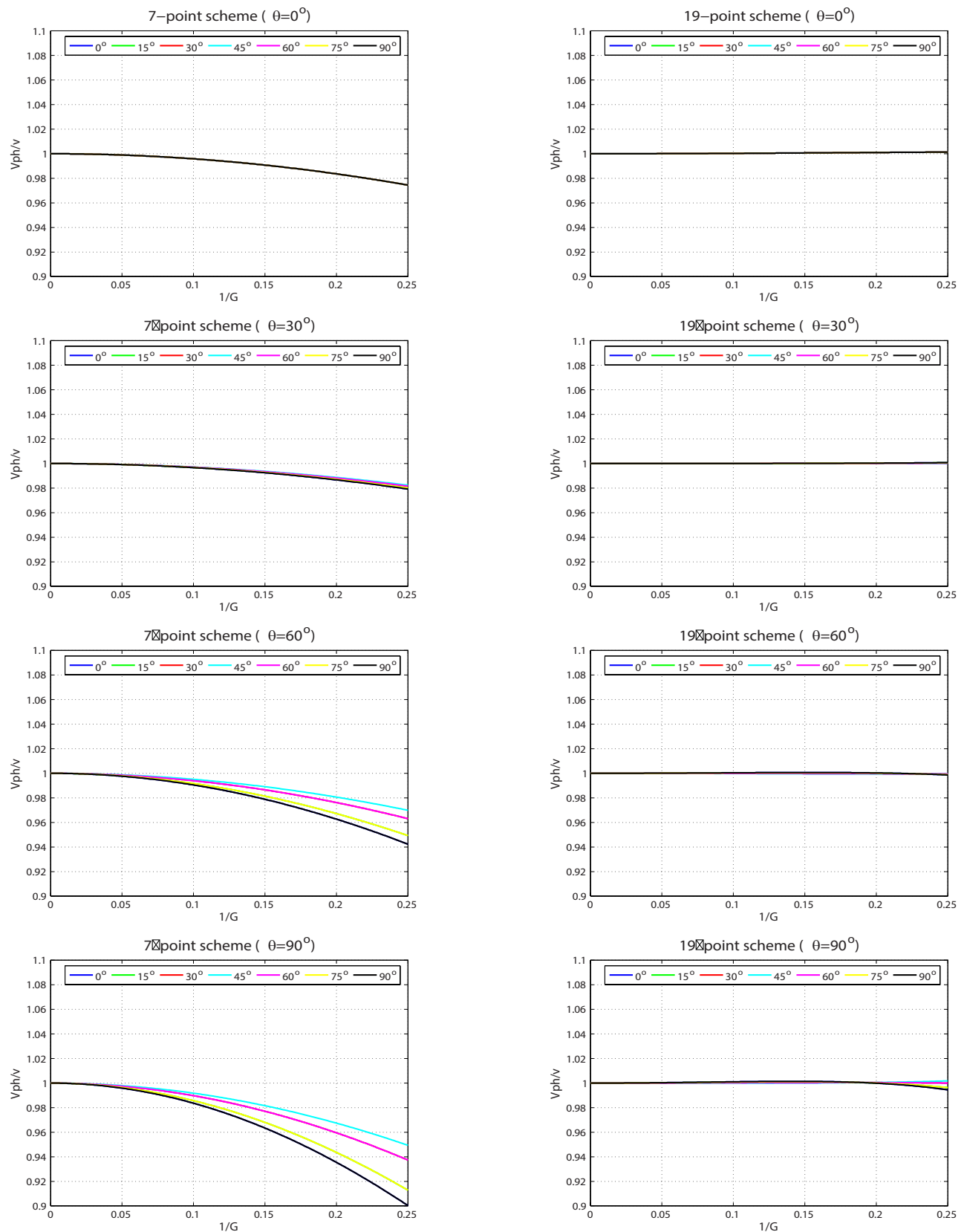


Figure 6: Normalized phase velocity curves of the classical 7-point scheme and the average-derivative optimal 19-point scheme for fixed propagation angle θ and different azimuth angles ϕ when $r_1 = 1$ and $r_2 = 2$.

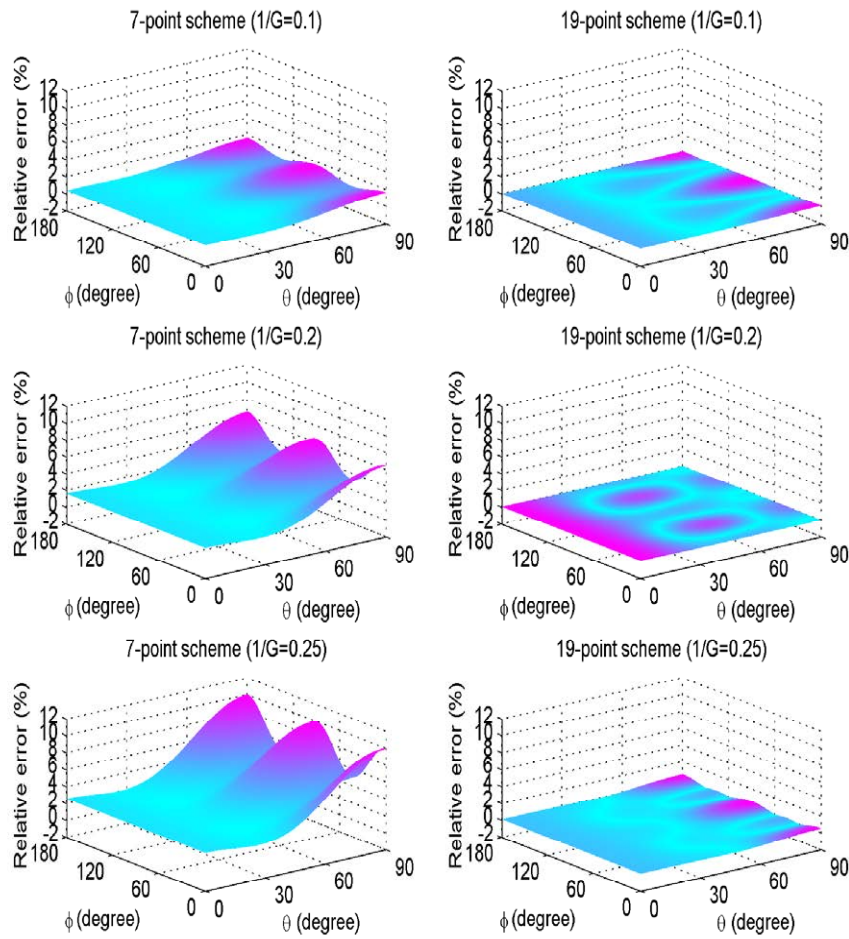


Figure 7: The relative phase velocity errors for the classical 7-point scheme and the average-derivative optimal 19-point scheme for different $1/G$ when $r_1 = 1$ and $r_2 = 2$.

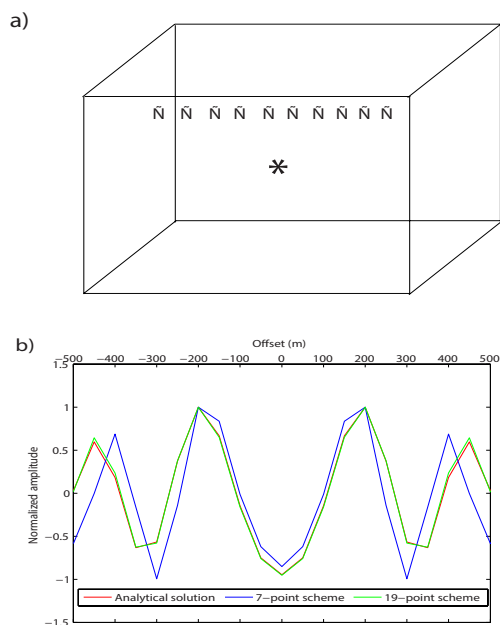


Figure 8: (a) The homogeneous model. “*” represents the source. “▽” represents the receiver. (b) Wavefields computed with the analytical method, the classical 7-point scheme, and the average-derivative optimal 19-point scheme.

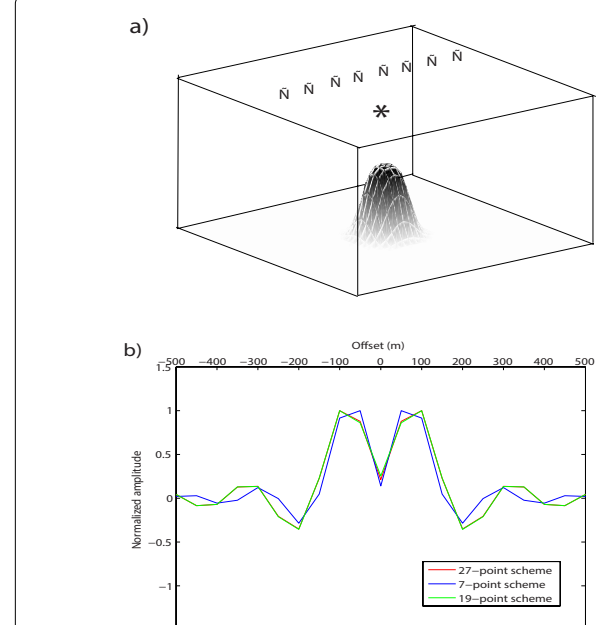


Figure 9: (a) The salt model. “*” represents the source. “▽” represents the receiver. (b) Wavefields computed with the average-derivative 27-point optimal scheme, the classical 7-point scheme, and the average-derivative optimal 19-point scheme.

of directional sampling intervals. Compared to the classical 7-point scheme, within the phase velocity error of 1%, this new 19-point optimal scheme reduces the number of per shortest wavelength from 13 to 4 for both equal and unequal directional sampling intervals. Two numerical examples confirm the theoretical analysis.

Acknowledgments

This work is supported by National Natural Science Foundation of China under grant Nos. 41474104 and 41274139.

References

1. Virieux J, Operto S (2009) An overview of full-waveform inversion in exploration geophysics: *Geophysics*, 74: WCC1-WCC26.
2. Tarantola A (1984) Inversion of seismic reflection data in the acoustic approximation: *Geophysics*, 49: 1259-1266.
3. Gauthier O, Virieux J, Tarantola A (1986) Two-dimensional nonlinear inversion of seismic waveforms: Numerical results: *Geophysics*, 51: 1387-1403.
4. Boonyasirwat C, Valasek P, Routh P, Cao W, Schuster GT, et al. (2009) An efficient multiscale method for time-domain waveform tomography: *Geophysics*, 74: WCC59-WCC68.
5. Pratt RG, Worthington MH (1990) Inverse theory applied to multi-source cross-hole tomography, Part I: acoustic wave-equation method: *Geophysical Prospecting*, 38: 287-310.
6. Pratt RG, Shin C, Hicks GJ (1998) Gauss-Newton and full New-ton methods in frequency-space seismic waveform inversion: *Geophysical Journal International*, 133: 341-362.
7. Brenders AJ, Pratt RG (2007) Full waveform tomography for litho-spheric imaging: results from a blind test in a realistic crustal model: *Geophysical Journal International*, 168: 133-151.
8. Chen JB (2009) Lax-Wendroff and Nyström methods for seismic modelling: *Geophysical Prospecting*, 57: 931-941.
9. Jo CH, Shin C, Suh JH (1996) An optimal 9-point, finite-difference, frequency-space, 2-D scalar wave extrapolator: *Geophysics*, 61: 529-537.
10. Symes WM (2007) Reverse-time migration with optimal checkpointing: *Geophysics*, 72: SM213-SM221.
11. Clapp RG (2009) Reverse time migration with random boundaries: 79th Annual International Meeting, SEG, Expanded Abstracts, Pp: 2809-2813.
12. Hustedt B, Operto S, Virieux J (2004) Mix-grid and staggered-grid finite-difference methods for frequency-domain acoustic wave modelling: *Geophysical Journal International*, 157: 1269-1296.
13. Operto S, Virieux J, Amestoy P, L'Excellent JY, Giraud L, et al. (2007a) 3D finite-difference frequency-domain modeling of visco-acoustic wave propagation using a massively parallel direct solver: A feasibility study: *Geophysics*, 72: SM195-SM211.
14. Chen JB (2012) An average-derivative optimal scheme for frequency-domain scalar wave equation: *Geophysics*, 77: T201-T210.
15. Chen JB (2001) New schemes for the nonlinear Schrodinger equation: *Applied Mathematics and Computation*, 124: 371-379.
16. Chen JB (2008) Variational integrators and the finite element method: *Applied Mathematics and Computation*, 196: 941-958.
17. Chen JB (2014) A 27-point scheme for 3D frequency-domain scalar wave equation based on an average-derivative method: *Geophysical Prospecting*, 62: 258-277.